IEEE Access
Multidisciplinary | Rapid Review | Open Access Journal

SPECIAL SECTION ON RECONFIGURABLE INTELLIGENT SURFACE AIDED COMMUNICATIONS FOR 6G AND BEYOND

Received May 6, 2021, accepted May 28, 2021, date of publication June 3, 2021, date of current version June 11, 2021.

Digital Object Identifier 10.1109/ACCESS.2021.3086067

On Performance of Two-Way Full-Duplex Communication System With Reconfigurable Intelligent Surface

BA CAO NGUYEN[1,2], TRAN MANH HOANG[3], LE THE DUNG[1,4], (Member, IEEE), AND TAEJOON KIM[1], (Member, IEEE)

[1]School of Information and Communication Engineering, Chungbuk National University, Cheongju 28644, South Korea
[2]Faculty of Basic Techniques, Telecommunications University, Nha Trang 65000, Vietnam
[3]Faculty of Telecommunications Services, Telecommunications University, Nha Trang 65000, Vietnam
[4]Department of Technology, Dong Nai Technology University, Bien Hoa 810000, Vietnam

Corresponding author: Taejoon Kim (ktjcc@chungbuk.ac.kr)

This work was supported by the Basic Science Research Program through the National Research Foundation of Korea (NRF) by the Ministry of Education under Grant 2020R1I1A3068305.

ABSTRACT In this paper, we apply a reconfigurable intelligent surface (RIS) to a two-way (TW) full-duplex (FD) wireless communication system, where a RIS has N reflecting elements and operates as a relay station forwarding signals between two FD terminals. To demonstrate the advantages of RIS compared with traditional relay, we also present the system and signal models of the TW-FD amplify-and-forward relay (AFR) system. We mathematically analyze the performance of the TW-FD-RIS system by deriving the exact closed-form expressions of the average outage probability (AOP) and the average symbol error rate (ASER) in the case $N = 1$, and approximate expressions of the AOP and the ASER in the case $N \geq 2$. Besides, we provide the exact closed-form expression of the AOP and approximate expression of the ASER of the TW-FD-AFR system. Monte-Carlo simulations validate all derived mathematical expressions. Numerical results demonstrate that using the RIS greatly improves the TW-FD communication system's performance compared with using amplify-and-forward (AF) relay. Specifically, even the RIS with one element ($N = 1$), the AOP and ASER of the TW-FD-RIS system are still lower than those of the TW-FD-AFR system in the low signal-to-noise ratio (SNR) regime. However, in the high SNR regime, the AOP and ASER of the TW-FD-RIS system are higher. In the case $N \geq 2$, the AOP and ASER of the TW-FD-RIS system are significantly reduced. On the other hand, the impact of residual self-interference (SI) due to FD transmission mode on the performance of TW-FD-RIS and TW-FD-AFR systems is remarkable, making the AOP and ASER of these two systems reach the error floor in the high SNR regime. Fortunately, the usage of RIS with $N \geq 2$ can greatly reduce this impact and avoid the error floor for the TW-FD-RIS system.

INDEX TERMS Two-way full-duplex, reconfigurable intelligent surface, amplify-and-forward relay, average outage probability, average symbol error rate.

I. INTRODUCTION

Recently, smart radio environments are expected to enhance the coverage, quality, and reliability of wireless communication systems. Specifically, reflective surfaces such as reconfigurable intelligent surface (RIS), large intelligent surface (LIS), and intelligent reflective surface (IRS) have been introduced to assist wireless communication systems [1], [2]. In particular, by controlling the characteristics of reflection, refraction, and scattering of radio waves, RIS can provide better performance than the traditional relay techniques in terms of the outage probability (OP) and energy efficiency [1]–[4]. Additionally, unlike the traditional relay stations, RIS can operate without decoding, encoding, and radio frequency (RF) processing, leading to a significant reduction in the system complexity. Thus, RIS-assisted wireless communication systems become a promising solution that can be exploited in the sixth generation (6G) and beyond wireless networks [3], [5], [6].

On the other hand, full-duplex (FD) transmission is useful for the fifth generation (5G), 6G, and beyond networks. Particularly, FD can enhance the spectral efficiency (SE)

The associate editor coordinating the review of this manuscript and approving it for publication was A. Swindlehurst.

two times in comparison with conventional half-duplex (HD) transmission because FD transmission enables wireless devices to transmit and receive signals at the same time and on the same frequency band [7]–[9]. Consequently, FD transmission is expected to replace the conventional HD transmission in the near future because it satisfies the requirements of high-capacity wireless systems. However, the high power of residual self-interference (SI) after all self-interference cancellation (SIC) techniques is still a challenge for FD devices because the residual SI degrades the performance of FD wireless communication systems. Fortunately, recent reports about the SIC in FD devices demonstrated that SI could be greatly removed to make the residual SI power as low as the noise floor [10]–[13]. This positive result indicates that FD devices can be deployed in practical scenarios.

In recent reports, the RIS is exploited in wireless communication systems to illustrate its advantages in comparison with relay networks [1], [2], [14]. Specifically, the optimal phases at the RIS for maximizing the signal-to-interference-plus-noise ratio (SINR) in a two-way (TW) HD communication system were proposed in [1]. Then, the OP and SE expressions were derived to evaluate the performance of this HD-TW-RIS system. Their results showed that increasing the number of elements of RIS can significantly reduce the OP and increase the SE of the HD-TW-RIS system. In [2], a one-way (OW)-HD-RIS system was investigated in terms of the OP and the ergodic capacity (EC) compared with the amplify-and-forward (AF) relay (AFR) system. It clearly indicated that the OP performance of the OW-HD-RIS system could be higher than that of the HD-OW-AFR system even when the RIS is only equipped with one element. Also, the work in [14] claimed that the RIS could be applied in wireless communication systems at high-frequency bands such as millimeter wave (30-100 GHz) and sub-millimeter wave (greater than 100 GHz). Furthermore, using the RISs with a larger number of elements yielded a better data rate than using relay and reduced the implementation complexity.

The RIS-assisted wireless communication systems have been investigated through mathematical analysis and implementations in various scenarios. In [15], the RIS was used to assist device-to-device (D2D) communications. By deploying the RIS and optimizing phase shifts, the interference in the D2D communication system can be greatly reduced. The implementations of RIS on reflectarrays or metasurfaces were investigated in [16], and the OP of RIS-assisted wireless communication systems was derived in the case of hardware impairments [17] and non-orthogonal multiple access networks [18]–[20]. To investigate the reliable communication of wireless systems using the RIS, the work in [21] used OP expression. It demonstrated that RIS could provide better reliability with a larger number of elements in the RIS. In [22], the authors proposed the optimization problem that could maximize the signal-to-noise ratio (SNR) at the receiver in both active and passive beamforming cases. Also, the asymptotic OP of the system was derived over Rician fading channels. For improving the system performance, the RIS selection was applied in [23]. On the other hand, a RIS-assisted underwater optical communication system with a decode-and-forward (DF) relaying protocol was presented in [24]. Recently, exploiting RIS in FD communication systems was also performed in [25]–[27]. Specifically, the work of [26] illustrated that the FD technique could outperform the HD technique when combined with the RIS. In addition, the usage of the RIS in the TW-FD system can suppress the users' interference because the RIS can create effective reflecting paths between the base station and users [27].

From the above discussions, RIS-assisted wireless communication systems have a great potential for 6G and beyond networks. Importantly, the RIS can assist TW communication systems with FD users. Meanwhile, most of the previous works exploiting the RIS in OW and HD systems. Therefore, in this work, we mathematically investigate the advantages of using the RIS in a TW-FD system and compare with those in the TW-FD-AFR system. The main contributions of this paper are summarized as follows:

- We consider a RIS-assisted TW-FD system (called a TW-FD-RIS system) where two terminals are FD devices and the RIS has N reflecting elements for reflecting bidirectional communication. Specifically, we also examine a TW-FD-AFR system with an FD-AF relay. The cases of imperfect SIC at two terminals of the TW-FD-RIS system and at three nodes in the TW-FD-AFR system are investigated.
- We calculate the signal-to-interference-plus-noise ratios (SINRs) of the TW-FD-RIS and TW-FD-AFR systems with residual SI and then use them to obtain the expressions of the average OP (AOP) and the average SER (ASER) over Rayleigh fading channels. Specifically, the AOP and ASER of the TW-FD-RIS system in the case $N = 1$ and the AOP of the TW-FD-AFR system are exact closed-form expressions. Meanwhile, the AOP and ASER of the TW-FD-RIS system in the case $N \geq 2$ and the ASER of the TW-FD-AFR system are approximate expressions. We validate all these derived expressions via Monte-Carlo simulations.
- We analyze and compare the performance of the two systems in various scenarios. In particular, we find that the performance in terms of the AOP and ASER of the TW-FD-RIS system in the case $N = 1$ is better in the low SNR regime and worse in the high SNR regime than those of the TW-FD-AFR system. In the case $N \geq 2$, the TW-FD-RIS system's performance is significantly higher than that of the TW-FD-AFR system. Also, the influence of the residual SI on the performance of these two systems is significant. The AOPs and ASERs of the TW-FD-RIS and TW-FD-AFR systems reach the error floors in the high SNR regime. Fortunately, the usage of two or more than two elements in RIS can greatly reduce the impact of residual SI and significantly improve the TW-FD-RIS system's performance.

The rest of this paper is organized as follows. Section II presents the system and signal models of TW-FD-RIS and TW-FD-AFR systems. Section III analyzes the performance in terms of the AOP and ASER of TW-FD-RIS and TW-FD-AFR systems over Rayleigh fading channels. Section IV provides numerical results obtained from several evaluation scenarios and discusses these results' features. Finally, Section V concludes the paper.

II. SYSTEM MODEL

This section provides the system and signal models of the TW-FD-RIS system in detail and compares them with those of the TW-FD-AFR system. Specifically, the received signals and signal processing at all terminals are clearly explained for both TW-FD-RIS and TW-FD-AFR systems. Then, the end-to-end signal-to-interference-plus-noise ratios (SINRs) at terminals are derived for further analysis.

A. TW-FD-RIS SYSTEM

Fig. 1 presents the model of the TW-FD-RIS system where two terminals, A and B, exchange data via a RIS. The RIS has N reflecting elements (or metasurfaces). Due to far distance and deep fading, the direct link between A and B is not available. In particular, A and B are FD devices and equipped with two antennas for transmitting and receiving signals separately. Since FD operating mode is exploited, A and B suffer from the self-interference (SI) induced from their transmitting antennas to receiving antennas. Additionally, they also suffer from the SI due to the RIS, i.e., the RIS reflects the transmitted signals from the transmitting antennas of A and B to the receiving antennas of A and B, respectively.

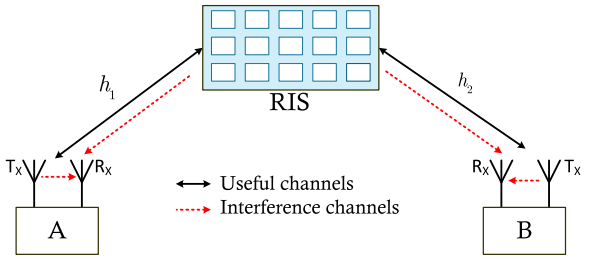

FIGURE 1. Illustration of the TW-FD-RIS system.

At one time slot and the same frequency band, the received signals at A and B through the RIS are, respectively, given as

$$y_{\mathrm{A}} = \sum_{n=1}^{N} h_{\mathrm{BS}_n} h_{\mathrm{S}_n\mathrm{A}} \exp(j\phi_n) s_{\mathrm{B}} + \tilde{h}_{\mathrm{AA}} s_{\mathrm{A}} + \sum_{n=1}^{N} h_{\mathrm{AS}_n} h_{\mathrm{S}_n\mathrm{A}} \exp(j\phi_n) s_{\mathrm{A}} + z_{\mathrm{A}}, \quad (1)$$

$$y_{\mathrm{B}} = \sum_{n=1}^{N} h_{\mathrm{AS}_n} h_{\mathrm{S}_n\mathrm{B}} \exp(j\phi_n) s_{\mathrm{A}} + \tilde{h}_{\mathrm{BB}} s_{\mathrm{B}} + \sum_{n=1}^{N} h_{\mathrm{BS}_n} h_{\mathrm{S}_n\mathrm{B}} \exp(j\phi_n) s_{\mathrm{B}} + z_{\mathrm{B}}, \quad (2)$$

where h_{AS_n} and h_{BS_n} are, respectively, the fading coefficients of the channels from A and B to the n-th element of the RIS; $h_{\mathrm{S}_n\mathrm{A}}$ and $h_{\mathrm{S}_n\mathrm{B}}$ are, respectively, the fading coefficients of the channels from the n-th element of the RIS to A and B; ϕ_n is the phase shift induced by the n-th element of the RIS; s_{A} and s_{B} are, respectively, the transmitted signals from A and B with the average transmission power of P_{A} and P_{B}; $\tilde{h}_{\mathrm{AA}}$ and $\tilde{h}_{\mathrm{BB}}$ are, respectively, the fading coefficients of the SI channels from the transmitting antenna to the receiving antenna of A and from the transmitting antenna to the receiving antenna of B; the Gaussian noises at A and B with zero mean and variance of σ^2, i.e., $z_{\mathrm{A}} \sim \mathcal{CN}(0, \sigma_{\mathrm{A}}^2)$ and $z_{\mathrm{B}} \sim \mathcal{CN}(0, \sigma_{\mathrm{B}}^2)$. It is worth noticing that, to emphasize the SI component that is reflected by the RIS, the SI in this paper is presented in two terms, i.e., $\tilde{h}_{\mathrm{BB}} s_{\mathrm{B}}$ and $\sum_{n=1}^{N} h_{\mathrm{BS}_n} h_{\mathrm{S}_n\mathrm{B}} \exp(j\phi_n) s_{\mathrm{B}}$ in (2). This method was used in the literature such as in [1], [25]. Meanwhile, another different method is to aggregate all SIs in one term when presenting the received signals.

From (1) and (2), it is noted that the mathematical equations of the received signals at A and B are identical. Thus, in the following parts, we only derive the SINR, AOP, and ASER expressions at B. These expressions at A can be obtained similarly.

After receiving signal, B applies all SIC techniques to reduce the SI power including the terms $\tilde{h}_{\mathrm{BB}} s_{\mathrm{B}}$ and $\sum_{n=1}^{N} h_{\mathrm{BS}_n} h_{\mathrm{S}_n\mathrm{B}} \exp(j\phi_n) s_{\mathrm{B}}$ in (2). Since B knows its transmitted signal s_{B}, it can totally remove the direct path from its transmitting antenna to receiving antenna. However, it is too difficult to completely suppress the SI signals induced by the reflected paths from the transmitting antenna of B to surrounding objects (including the RIS) then back to the receiving antenna of B. As a result, although three interference cancellation schemes are used together in space (propagation) domain, analog domain, and digital domain, the residual SI still exists in the system and distorts the intended signal. Specifically, the solutions presented in [10] provided an attenuation level of 45 dB in the analog domain and 50 dB in the digital domain. According to [10], an attenuation of more than 110 dB in the propagation domain helps convert the SI into the noise floor. Consequently, it is reasonable to model the residual SI as a noise source. Furthermore, many works in the literature have assumed that the residual SI follows Gaussian distribution [28]–[31]. Thus, in this paper, we also consider the residual SI as Gaussian noise. In addition, since the three interference cancellation schemes are used, the phase shifts in the SI caused by the RIS can be completely removed after doing SIC in the digital domain because the digital-domain cancellation is carried out after a quantization operation [1], [25]. Specifically, after applying all SIC techniques, the residual SI at B (denoted by I_{B}) is expressed as $I_{\mathrm{B}} \sim \mathcal{CN}(0, k_{\mathrm{B}}^2 P_{\mathrm{B}})$, where k_{B} refers to the residual SI level at B.

Then, (2) becomes

$$y_{\mathrm{B}} = \sum_{n=1}^{N} h_{\mathrm{AS}_n} h_{\mathrm{S}_n\mathrm{B}} \exp(j\phi_n) s_{\mathrm{A}} + I_{\mathrm{B}} + z_{\mathrm{B}}. \quad (3)$$

Note that the RIS-related fading coefficients h_{AS_n} and $h_{\mathrm{S}_n\mathrm{B}}$ are, respectively, given by [1]–[3]

$$h_{\mathrm{AS}_n} = a_{\mathrm{AS}_n} \exp(-j\psi_{\mathrm{AS}_n}), \tag{4}$$

$$h_{\mathrm{S}_n\mathrm{B}} = a_{\mathrm{S}_n\mathrm{B}} \exp(-j\psi_{\mathrm{S}_n\mathrm{B}}), \tag{5}$$

where a_{AS_n} and $a_{\mathrm{S}_n\mathrm{B}}$ are the magnitudes and ψ_{AS_n} and $\psi_{\mathrm{S}_n\mathrm{B}}$ are the phases of h_{AS_n} and $h_{\mathrm{S}_n\mathrm{B}}$, respectively.

Therefore, from (3), the instantaneous SINR at B is computed as

$$\gamma_{\mathrm{B}}^{\mathrm{RIS}} = \frac{\left| \sum_{n=1}^{N} a_{\mathrm{AS}_n} a_{\mathrm{S}_n\mathrm{B}} \exp\left(j(\phi_n - \psi_{\mathrm{AS}_n} - \psi_{\mathrm{S}_n\mathrm{B}})\right) \right|^2 P_{\mathrm{A}}}{k_{\mathrm{B}}^2 P_{\mathrm{B}} + \sigma_{\mathrm{B}}^2}. \tag{6}$$

Additionally, ϕ_n can be chosen as the optimal value that maximizes the SINR in the receivers [1], [2]. In other words, the RIS can adjust its phase to maximize the received signal power at each terminal because it knows the global phase information [1], [2], [32], i.e.,

$$\phi_n = \psi_{\mathrm{AS}_n} + \psi_{\mathrm{S}_n\mathrm{B}}. \tag{7}$$

Therefore, the maximum instantaneous SINR at B becomes

$$\gamma_{\mathrm{B}}^{\mathrm{RIS}} = \frac{\left| \sum_{n=1}^{N} a_{\mathrm{AS}_n} a_{\mathrm{S}_n\mathrm{B}} \right|^2 P_{\mathrm{A}}}{k_{\mathrm{B}}^2 P_{\mathrm{B}} + \sigma_{\mathrm{B}}^2}. \tag{8}$$

B. TW-FD-AFR SYSTEM

Fig. 2 illustrates the system model of a TW-FD-AFR system where two terminals, A and B, exchange data via the assistance of a relay (R). Specifically, A, B, and R are FD devices equipped with two antennas for transmitting and receiving signals separately. Similar to the TW-FD-RIS system, A, B, and R have to apply all SIC techniques to reduce the SI power.

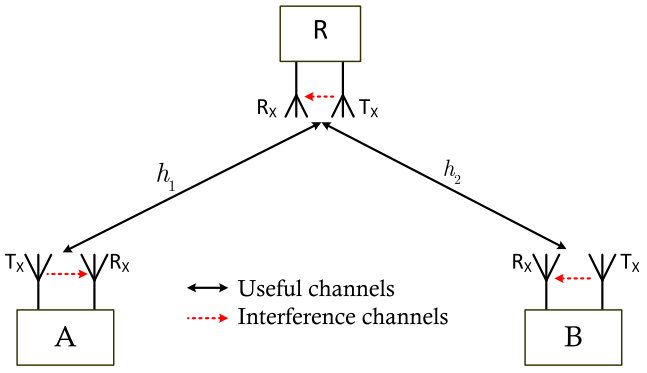

FIGURE 2. Illustration of the TW-FD-AFR system.

At one time slot, the received signals at R are expressed as

$$y_{\mathrm{R}} = h_{\mathrm{AR}} s_{\mathrm{A}} + h_{\mathrm{BR}} s_{\mathrm{B}} + \tilde{h}_{\mathrm{RR}} s_{\mathrm{R}} + z_{\mathrm{R}}, \tag{9}$$

where h_{AR} and h_{BR} are, respectively, the fading coefficients of the channels from A and B to R; $\tilde{h}_{\mathrm{RR}}$ is the SI from the transmitting antenna to the receiving antenna of R; s_{R} is the transmitted signal from R with the average transmission power of P_{R}; z_{R} is the Gaussian noise at R with zero mean and variance of σ^2, i.e., $z_{\mathrm{R}} \sim \mathcal{CN}(0, \sigma_{\mathrm{R}}^2)$.

As mentioned earlier, after R applies all SIC techniques to remove the SI, the residual SI at R (denoted by I_{R}) is expressed as $I_{\mathrm{R}} \sim \mathcal{CN}(0, k_{\mathrm{R}}^2 P_{\mathrm{R}})$, where k_{R} represents the residual SI level at R.

Then, the received signal at R is given by

$$y_{\mathrm{R}} = h_{\mathrm{AR}} s_{\mathrm{A}} + h_{\mathrm{BR}} s_{\mathrm{B}} + I_{\mathrm{R}} + z_{\mathrm{R}}. \tag{10}$$

Next, R amplifies its received signals and transmits them to A and B. Mathematically, the transmitted signal of R is presented as

$$s_{\mathrm{R}} = G y_{\mathrm{R}}, \tag{11}$$

where G is the relaying gain which is calculated as

$$G = \sqrt{\frac{P_{\mathrm{R}}}{|h_{\mathrm{AR}}|^2 P_{\mathrm{A}} + |h_{\mathrm{BR}}|^2 P_{\mathrm{B}} + k_{\mathrm{R}}^2 P_{\mathrm{R}} + \sigma_{\mathrm{R}}^2}}. \tag{12}$$

Similar to the TW-FD-RIS system, we focus on the received signal at B in the TW-FD-AFR system. The received signal and other expressions at A can be easily obtained by using similar calculations. The received signal at B after applying all SIC techniques is

$$y_{\mathrm{B}} = h_{\mathrm{RB}} s_{\mathrm{R}} + I_{\mathrm{B}} + z_{\mathrm{B}}. \tag{13}$$

Using (10) and (11), the received signal at B becomes

$$\begin{aligned} y_{\mathrm{B}} &= h_{\mathrm{RB}} G y_{\mathrm{R}} + I_{\mathrm{B}} + z_{\mathrm{B}} \\ &= h_{\mathrm{RB}} G\Big(h_{\mathrm{AR}} s_{\mathrm{A}} + h_{\mathrm{BR}} s_{\mathrm{B}} + I_{\mathrm{R}} + z_{\mathrm{R}}\Big) + I_{\mathrm{B}} + z_{\mathrm{B}}. \end{aligned} \tag{14}$$

By utilizing a suitable network coding scheme, B can totally remove its transmitted signal s_{B} from y_{B} [33]. Now, the received signal at B is expressed as

$$y_{\mathrm{B}} = h_{\mathrm{RB}} G\Big(h_{\mathrm{AR}} s_{\mathrm{A}} + I_{\mathrm{R}} + z_{\mathrm{R}}\Big) + I_{\mathrm{B}} + z_{\mathrm{B}}. \tag{15}$$

From (15), the SINR at B in the TW-FD-AFR system is determined as

$$\begin{aligned} \gamma_{\mathrm{B}}^{\mathrm{AFR}} &= \frac{|h_{\mathrm{RB}}|^2 |h_{\mathrm{AR}}|^2 P_{\mathrm{A}}}{|h_{\mathrm{RB}}|^2 (k_{\mathrm{R}}^2 P_{\mathrm{R}} + \sigma_{\mathrm{R}}^2) + (k_{\mathrm{B}}^2 P_{\mathrm{B}} + \sigma_{\mathrm{B}}^2)/G^2} \\ &= \frac{|h_{\mathrm{AR}}|^2 |h_{\mathrm{RB}}|^2 P_{\mathrm{A}} P_{\mathrm{R}}}{|h_{\mathrm{AR}}|^2 X_{\mathrm{B}} P_{\mathrm{A}} + |h_{\mathrm{RB}}|^2 (X_{\mathrm{R}} P_{\mathrm{R}} + X_{\mathrm{B}} P_{\mathrm{B}}) + X_{\mathrm{R}} X_{\mathrm{B}}}, \end{aligned} \tag{16}$$

where $X_{\mathrm{R}} = k_{\mathrm{R}}^2 P_{\mathrm{R}} + \sigma_{\mathrm{R}}^2$ and $X_{\mathrm{B}} = k_{\mathrm{B}}^2 P_{\mathrm{B}} + \sigma_{\mathrm{B}}^2$ are, respectively, the interference-plus-noises at R and B.

III. PERFORMANCE ANALYSIS

A. TW-FD-RIS SYSTEM

1) AVERAGE OUTAGE PROBABILITY ANALYSIS

The outage probability of wireless systems is defined as the probability that the instantaneous data transmission rate is

lower than a pre-defined data transmission rate [34]. Mathematically, the AOP of the TW-FD-RIS system (denoted by $\mathcal{P}_{\text{out}}^{\text{RIS}}$) is calculated as

$$\mathcal{P}_{\text{out}}^{\text{RIS}} = \Pr\{\log_2(1+\gamma_{\text{B}}^{\text{RIS}}) < \mathcal{R}\}, \tag{17}$$

where $\gamma_{\text{B}}^{\text{RIS}}$ is given in (8); $\mathcal{R}$ is the pre-data transmission rate of the considered TW-FD-RIS system.

We can rewrite (17) as

$$\mathcal{P}_{\text{out}}^{\text{RIS}} = \Pr\{\gamma_{\text{B}}^{\text{RIS}} < 2^{\mathcal{R}}-1\} = \Pr\{\gamma_{\text{B}}^{\text{RIS}} < \gamma_{\text{th}}\}, \tag{18}$$

where $\gamma_{\text{th}} = 2^{\mathcal{R}}-1$ is the SINR threshold.

Replacing $\gamma_{\text{B}}^{\text{RIS}}$ from (8) into (18), we have

$$\begin{aligned}\mathcal{P}_{\text{out}}^{\text{RIS}} &= \Pr\left\{\frac{\left|\sum_{n=1}^{N} a_{\text{AS}_n} a_{\text{S}_n\text{B}}\right|^2 P_{\text{A}}}{k_{\text{B}}^2 P_{\text{B}} + \sigma_{\text{B}}^2} < \gamma_{\text{th}}\right\} \\ &= \Pr\left\{\frac{\left|\sum_{n=1}^{N} a_{\text{AS}_n} a_{\text{S}_n\text{B}}\right|^2 P_{\text{A}}}{X_{\text{B}}} < \gamma_{\text{th}}\right\}. \end{aligned} \tag{19}$$

It is equivalent to

$$\mathcal{P}_{\text{out}}^{\text{RIS}} = \Pr\left\{\sum_{n=1}^{N} a_{\text{AS}_n} a_{\text{S}_n\text{B}} < \sqrt{\frac{X_{\text{B}}\gamma_{\text{th}}}{P_{\text{A}}}}\right\}. \tag{20}$$

From (20), the AOP of the TW-FD-RIS system is computed in the following Theorem 1.

Theorem 1: The AOP of the TW-FD-RIS system is approximated as

$$\mathcal{P}_{\text{out}}^{\text{RIS}} \approx 1 - \frac{\Gamma\left(\frac{N\pi^2}{16-\pi^2}, \frac{4\pi}{16-\pi^2}\sqrt{\frac{X_{\text{B}}\gamma_{\text{th}}}{P_{\text{A}}}}\right)}{\Gamma\left(\frac{N\pi^2}{16-\pi^2}\right)}, \tag{21}$$

where $\Gamma(.,.)$ and $\Gamma(.)$ are, respectively, the upper incomplete gamma function and the gamma function that satisfy $\Gamma(a,x)+\gamma(a,x) = \Gamma(a)$, where γ is the lower incomplete gamma function.

Proof: Applying [1, Eq. (22)], the AOP of TW-FD-RIS system in the case $N \geq 2$ in (20) is now calculated as

$$\mathcal{P}_{\text{out}}^{\text{RIS}} \approx \frac{1}{\Gamma\left(\frac{N\pi^2}{16-\pi^2}\right)}\gamma\left(\frac{N\pi^2}{16-\pi^2}, \frac{4\pi}{16-\pi^2}\sqrt{\frac{X_{\text{B}}\gamma_{\text{th}}}{P_{\text{A}}}}\right). \tag{22}$$

Then, using $\Gamma(a,x)+\gamma(a,x) = \Gamma(a)$, we can easily obtain the AOP expression of TW-FD-RIS system as (21).

Since the approximations of gamma and incomplete gamma functions in the extreme conditions cause great errors, the asymptotic expression of the AOP was not provided in this paper.

In the special case, i.e., $N = 1$, we can achieve the exact closed-form expression of the AOP of TW-FD-RIS system in the following Lemma 1.

Lemma 1: The exact closed-form expression of the AOP of TW-FD-RIS system for $N = 1$ is given by

$$\mathcal{P}_{\text{out}}^{\text{RIS}} = 1 - \sqrt{\frac{4\,X_{\text{B}}\gamma_{\text{th}}}{P_{\text{A}}}}\mathcal{K}_1\left(\sqrt{\frac{4\,X_{\text{B}}\gamma_{\text{th}}}{P_{\text{A}}}}\right), \tag{23}$$

where $\mathcal{K}_1(.)$ the first-order modified Bessel function of the second kind.

Proof: In the case $N = 1$, (20) becomes

$$\begin{aligned}\mathcal{P}_{\text{out}}^{\text{RIS}} &= \Pr\left\{a_{\text{AS}}a_{\text{SB}} < \sqrt{\frac{X_{\text{B}}\gamma_{\text{th}}}{P_{\text{A}}}}\right\} \\ &= \Pr\left\{|a_{\text{AS}}|^2|a_{\text{SB}}|^2 < \frac{X_{\text{B}}\gamma_{\text{th}}}{P_{\text{A}}}\right\}. \end{aligned} \tag{24}$$

Since $|a_{\text{AS}}|^2$ and $|a_{\text{SB}}|^2$ are two instantaneous magnitudes which follow Rayleigh distributions, applying [35, Eq. (18)], we can obtain the AOP expression of TW-FD-RIS system in the case $N = 1$ as (23).

2) AVERAGE SYMBOL ERROR RATE ANALYSIS

The ASER at B in the TW-FD-RIS system is calculated as

$$\begin{aligned}\text{SER}_{\text{B}}^{\text{RIS}} &= \alpha\mathbb{E}\{Q(\sqrt{\beta\gamma_{\text{B}}^{\text{RIS}}})\} \\ &= \frac{\alpha}{\sqrt{2\pi}}\int_0^{\infty} F_{\gamma_{\text{B}}^{\text{RIS}}}\left(\frac{t^2}{\beta}\right)\exp\left(-\frac{t^2}{2}\right)dt, \end{aligned} \tag{25}$$

where $\mathbb{E}$ is the expectation operator; α and β are constants whose values depend on the modulation types, e.g., $\alpha = 1$, $\beta = 2$ for the binary phase-shift keying (BPSK) modulation and $\alpha = 2$, $\beta = 1$ for the 4-quadrature amplitude modulation (4-QAM); $Q(x) = \frac{1}{\sqrt{2\pi}}\int_x^{\infty} e^{-t^2/2}dt$ is the Gaussian function; $F(.)$ is the cumulative distribution function (CDF) of $\gamma_{\text{B}}^{\text{RIS}}$. Let $x = t^2/\beta$ be a new variable, (25) is rewritten as

$$\text{SER}_{\text{B}}^{\text{RIS}} = \frac{\alpha\sqrt{\beta}}{2\sqrt{2\pi}}\int_0^{\infty}\frac{\exp\left(-\frac{\beta x}{2}\right)}{\sqrt{x}}F_{\gamma_{\text{B}}^{\text{RIS}}}(x)dx. \tag{26}$$

From (26), the $\text{SER}_{\text{B}}^{\text{RIS}}$ of the TW-FD-RIS system is derived in the following Theorem 2.

Theorem 2: The ASER of the TW-FD-RIS system is approximated as

$$\begin{aligned}\text{SER}_{\text{B}}^{\text{RIS}} \approx \frac{\alpha\sqrt{\beta}}{2\sqrt{2\pi}}\Bigg[\sqrt{\frac{2\pi}{\beta}} - \frac{\pi}{2M}\sum_{m=1}^{M}\sqrt{\frac{2(1-\phi_m^2)}{\beta[\ln 2 - \ln(1+\phi_m)]}} \\ \times\frac{\Gamma\left(\frac{N\pi^2}{16-\pi^2}, \frac{4\pi}{16-\pi^2}\sqrt{\frac{2\,X_{\text{B}}[\ln 2-\ln(1+\phi_m)]}{\beta P_{\text{A}}}}\right)}{\Gamma\left(\frac{N\pi^2}{16-\pi^2}\right)}\Bigg], \end{aligned} \tag{27}$$

where M is the complexity-accuracy trade-off parameter; $\phi_m = \cos\left(\frac{(2m-1)\pi}{2M}\right)$.

Proof: To obtain the ASER of the TW-FD-RIS system, we have to derive $F_{\gamma_{\rm B}^{\rm RIS}}(x)$ first and then replace it into (26). Based on the definition of the CDF of $\gamma_{\rm B}^{\rm RIS}$, i.e.,

$$F_{\gamma_{\rm B}^{\rm RIS}}(x) = \Pr\left\{\gamma_{\rm B}^{\rm RIS} < x\right\}, \tag{28}$$

we can easily derive $F_{\gamma_{\rm B}^{\rm RIS}}(x)$ from (21) as

$$F_{\gamma_{\rm B}^{\rm RIS}}(x) \approx 1 - \frac{\Gamma\left(\frac{N\pi^2}{16-\pi^2}, \frac{4\pi}{16-\pi^2}\sqrt{\frac{X_{\rm B}x}{P_{\rm A}}}\right)}{\Gamma\left(\frac{N\pi^2}{16-\pi^2}\right)}. \tag{29}$$

Replacing (29) into (26), the ASER is then computed as

$$\begin{aligned}
{\rm SER}_{\rm B}^{\rm RIS} &\approx \frac{\alpha\sqrt{\beta}}{2\sqrt{2\pi}} \int_0^\infty \frac{\exp\left(-\frac{\beta x}{2}\right)}{\sqrt{x}} \\
&\quad \times \left[1 - \frac{\Gamma\left(\frac{N\pi^2}{16-\pi^2}, \frac{4\pi}{16-\pi^2}\sqrt{\frac{X_{\rm B}x}{P_{\rm A}}}\right)}{\Gamma\left(\frac{N\pi^2}{16-\pi^2}\right)}\right] dx \\
&= \frac{\alpha\sqrt{\beta}}{2\sqrt{2\pi}}\Bigg[\int_0^\infty \frac{\exp\left(-\frac{\beta x}{2}\right)}{\sqrt{x}} dx \\
&\quad - \int_0^\infty \frac{\exp\left(-\frac{\beta x}{2}\right)\Gamma\left(\frac{N\pi^2}{16-\pi^2}, \frac{4\pi}{16-\pi^2}\sqrt{\frac{X_{\rm B}x}{P_{\rm A}}}\right)}{\Gamma\left(\frac{N\pi^2}{16-\pi^2}\right)\sqrt{x}} dx\Bigg].
\end{aligned} \tag{30}$$

Applying [36, Eq. (3.361.2)], the first integral in (30) is solved as

$$\int_0^\infty \frac{\exp\left(-\frac{\beta x}{2}\right)}{\sqrt{x}} dx = \sqrt{\frac{2\pi}{\beta}}. \tag{31}$$

To solve the second integral in (30), we change variable, i.e., $y = \exp(-\frac{\beta x}{2})$. Then, the second integral in (30) becomes

$$\begin{aligned}
&\int_0^\infty \frac{\exp\left(-\frac{\beta x}{2}\right)\Gamma\left(\frac{N\pi^2}{16-\pi^2}, \frac{4\pi}{16-\pi^2}\sqrt{\frac{X_{\rm B}x}{P_{\rm A}}}\right)}{\Gamma\left(\frac{N\pi^2}{16-\pi^2}\right)\sqrt{x}} dx \\
&= -\int_1^0 \frac{y\Gamma\left(\frac{N\pi^2}{16-\pi^2}, \frac{4\pi}{16-\pi^2}\sqrt{\frac{X_{\rm B}\frac{2}{\beta}\ln\frac{1}{y}}{P_{\rm A}}}\right)}{\Gamma\left(\frac{N\pi^2}{16-\pi^2}\right)\sqrt{\frac{2}{\beta}\ln\frac{1}{y}}} \frac{2\,dy}{\beta y} \\
&= \int_0^1 \frac{\sqrt{\frac{2}{\beta}\ln\frac{1}{y}}\Gamma\left(\frac{N\pi^2}{16-\pi^2}, \frac{4\pi}{16-\pi^2}\sqrt{\frac{X_{\rm B}\frac{2}{\beta}\ln\frac{1}{y}}{P_{\rm A}}}\right)}{\Gamma\left(\frac{N\pi^2}{16-\pi^2}\right)} dy.
\end{aligned} \tag{32}$$

Based on [37, Eq. (25.4.30)], the above integral yields

$$\begin{aligned}
&\int_0^1 \frac{\sqrt{\frac{2}{\beta}\ln\frac{1}{y}}\Gamma\left(\frac{N\pi^2}{16-\pi^2}, \frac{4\pi}{16-\pi^2}\sqrt{\frac{X_{\rm B}\frac{2}{\beta}\ln\frac{1}{y}}{P_{\rm A}}}\right)}{\Gamma\left(\frac{N\pi^2}{16-\pi^2}\right)} dy \\
&= \frac{\pi}{2M}\sum_{m=1}^{M}\sqrt{\frac{2(1-\phi_m^2)}{\beta[\ln 2 - \ln(1+\phi_m)]}} \\
&\quad \times \frac{\Gamma\left(\frac{N\pi^2}{16-\pi^2}, \frac{4\pi}{16-\pi^2}\sqrt{\frac{2\,X_{\rm B}[\ln 2 - \ln(1+\phi_m)]}{\beta P_{\rm A}}}\right)}{\Gamma\left(\frac{N\pi^2}{16-\pi^2}\right)}.
\end{aligned} \tag{33}$$

Plugging (31) and (33) into (30), we obtain the ASER of TW-FD-RIS system as (27) in Theorem 2.

In the special case, i.e., $N = 1$, we can represent the ASER of the TW-FD-RIS system through an exact closed-form expression in the following Lemma 2.

Lemma 2: The exact closed-form expression of ASER of TW-FD-RIS system for $N = 1$ is expressed as

$$\begin{aligned}
{\rm SER}_{\rm B}^{\rm RIS} = \frac{\alpha\sqrt{\beta}}{2\sqrt{2\pi}}\Bigg[&\sqrt{\frac{2\pi}{\beta}} - \sqrt{\frac{2}{\beta}}\Gamma\left(\frac{3}{3}\right)\Gamma\left(\frac{1}{2}\right)\exp\left(\frac{X_{\rm B}}{\beta P_{\rm A}}\right) \\
&\times \mathcal{W}_{-\frac{1}{2},\frac{1}{2}}\left(\frac{2\,X_{\rm B}}{\beta P_{\rm A}}\right)\Bigg],
\end{aligned} \tag{34}$$

where $\mathcal{W}$ is the Whittaker function.

Proof: By using (23), (28), and (29), we can obtain the exact expression of $F_{\gamma_{\rm B}^{\rm RIS}}(x)$ in the case $N = 1$. Thus, ${\rm SER}_{\rm B}^{\rm RIS}$ is calculated as

$$\begin{aligned}
{\rm SER}_{\rm B}^{\rm RIS} &= \frac{\alpha\sqrt{\beta}}{2\sqrt{2\pi}}\Bigg[\int_0^\infty \frac{\exp\left(-\frac{\beta x}{2}\right)}{\sqrt{x}} dx \\
&\quad - \int_0^\infty \frac{\exp\left(-\frac{\beta x}{2}\right)}{\sqrt{x}}\sqrt{\frac{4\,X_{\rm B}x}{P_{\rm A}}}\mathcal{K}_1\left(\sqrt{\frac{4\,X_{\rm B}x}{P_{\rm A}}}\right) dx\Bigg] \\
&= \frac{\alpha\sqrt{\beta}}{2\sqrt{2\pi}}\Bigg[\sqrt{\frac{2\pi}{\beta}} \\
&\quad - \sqrt{\frac{4\,X_{\rm B}}{P_{\rm A}}}\int_0^\infty \exp\left(-\frac{\beta x}{2}\right)\mathcal{K}_1\left(\sqrt{\frac{4\,X_{\rm B}x}{P_{\rm A}}}\right) dx\Bigg].
\end{aligned} \tag{35}$$

From [36, Eq. (6.643.3)], we have

$$\begin{aligned}
&\int_0^\infty \exp\left(-\frac{\beta x}{2}\right)\mathcal{K}_1\left(\sqrt{\frac{4\,X_{\rm B}x}{P_{\rm A}}}\right) dx \\
&= \frac{\Gamma\left(\frac{3}{3}\right)\Gamma\left(\frac{1}{2}\right)}{\sqrt{\frac{4\,X_{\rm B}}{P_{\rm A}}}}\sqrt{\frac{2}{\beta}}\exp\left(\frac{X_{\rm B}}{\beta P_{\rm A}}\right)\mathcal{W}_{-\frac{1}{2},\frac{1}{2}}\left(\frac{2\,X_{\rm B}}{\beta P_{\rm A}}\right).
\end{aligned} \tag{36}$$

Substituting (36) into (35), we obtain ${\rm SER}_{\rm B}^{\rm RIS}$ in the case $N = 1$ as (34) in Lemma 2.

3) ASYMPTOTIC SINR

To better show the impacts of the system parameters on the SINR at B of the considered TW-FD-RIS system, we elaborate this system in high SNR regime. Without loss of generality, we set $P_{\rm A} = P_{\rm B} = P$, $\sigma_{\rm A}^2 = \sigma_{\rm B}^2 = \sigma^2$, and ${\rm SNR} = P/\sigma^2$. In high SNR regime, the asymptotic expression of the SINR

in (8) can be computed as

$$\lim_{\mathrm{SNR}\to\infty}\gamma_{\mathrm{B}}^{\mathrm{RIS}} = \lim_{\mathrm{SNR}\to\infty}\frac{\left|\sum_{n=1}^{N} a_{\mathrm{AS}_n}a_{\mathrm{S}_n\mathrm{B}}\right|^2 P_{\mathrm{A}}}{k_{\mathrm{B}}^2 P_{\mathrm{B}}+\sigma_{\mathrm{B}}^2} = \lim_{\mathrm{SNR}\to\infty}\frac{\left|\sum_{n=1}^{N} a_{\mathrm{AS}_n}a_{\mathrm{S}_n\mathrm{B}}\right|^2 \frac{P}{\sigma^2}}{k_{\mathrm{B}}^2\frac{P}{\sigma^2}+1} = \lim_{\mathrm{SNR}\to\infty}\frac{\left|\sum_{n=1}^{N} a_{\mathrm{AS}_n}a_{\mathrm{S}_n\mathrm{B}}\right|^2 \mathrm{SNR}}{k_{\mathrm{B}}^2\mathrm{SNR}+1} = \frac{N}{k_{\mathrm{B}}^2}. \quad (37)$$

As shown in (37), in the high SNR regime, the end-to-end SINR at B of the considered TW-FD-RIS system depends on N (the number of reflecting elements) and k_{B}^2 (the residual SI level at B). For specific RIS and FD device, N and k_{B}^2 are constants; thus, the SINR is a constant in the high SNR regime. As a result, the AOP and ASER of the TW-FD-RIS system are also constants in the high SNR regime.

B. TW-FD-AFR SYSTEM

1) AVERAGE OUTAGE PROBABILITY ANALYSIS

Similar to the AOP of the TW-FD-RIS system, the AOP of the TW-FD-AFR system is calculated as

$$\mathcal{P}_{\mathrm{out}}^{\mathrm{AFR}} = \Pr\{\gamma_{\mathrm{B}}^{\mathrm{AFR}} < \gamma_{\mathrm{th}}\}. \quad (38)$$

Then, the AOP of the TW-FD-AFR system is derived in the following Theorem 3.

Theorem 3: The AOP of the TW-FD-AFR system over Rayleigh fading channels is computed as

$$\mathcal{P}_{\mathrm{out}}^{\mathrm{AFR}} = 1-2\exp\left(-\frac{(X_{\mathrm{R}}P_{\mathrm{R}}+X_{\mathrm{B}}P_{\mathrm{A}}+X_{\mathrm{B}}P_{\mathrm{B}})\gamma_{\mathrm{th}}}{P_{\mathrm{A}}P_{\mathrm{R}}}\right) \times\sqrt{\frac{X_{\mathrm{B}}(X_{\mathrm{R}}P_{\mathrm{R}}+X_{\mathrm{B}}P_{\mathrm{B}})\gamma_{\mathrm{th}}^2+X_{\mathrm{R}}X_{\mathrm{B}}P_{\mathrm{R}}\gamma_{\mathrm{th}}}{P_{\mathrm{A}}P_{\mathrm{R}}^2}} \times\mathcal{K}_1\left(2\sqrt{\frac{X_{\mathrm{B}}(X_{\mathrm{R}}P_{\mathrm{R}}+X_{\mathrm{B}}P_{\mathrm{B}})\gamma_{\mathrm{th}}^2+X_{\mathrm{R}}X_{\mathrm{B}}P_{\mathrm{R}}\gamma_{\mathrm{th}}}{P_{\mathrm{A}}P_{\mathrm{R}}^2}}\right). \quad (39)$$

Proof: From (38), $\mathcal{P}_{\mathrm{out}}^{\mathrm{AFR}}$ is expressed as

$$\mathcal{P}_{\mathrm{out}}^{\mathrm{AFR}} = 1-\int_0^{\infty}\left(1-F_{|h_{\mathrm{AR}}|^2}(\Delta)\right)f_{|h_{\mathrm{RB}}|^2}(z)dz, \quad (40)$$

where

$$\Delta = \frac{(X_{\mathrm{R}}P_{\mathrm{R}}+X_{\mathrm{B}}P_{\mathrm{B}})\gamma_{\mathrm{th}}}{P_{\mathrm{A}}P_{\mathrm{R}}} + \frac{X_{\mathrm{B}}(X_{\mathrm{R}}P_{\mathrm{R}}+X_{\mathrm{B}}P_{\mathrm{B}})\gamma_{\mathrm{th}}^2+X_{\mathrm{R}}X_{\mathrm{B}}P_{\mathrm{R}}\gamma_{\mathrm{th}}}{zP_{\mathrm{A}}P_{\mathrm{R}}^2};$$

$$z = |h_{\mathrm{RB}}|^2 - \frac{X_{\mathrm{B}}\gamma_{\mathrm{th}}}{P_{\mathrm{R}}};$$

$f(.)$ is the probability density function (PDF).

Since the Rayleigh fading channels are studied, the PDF and CDF of the instantaneous channel gain, i.e., $|h|^2$, are, respectively, given by

$$f_{|h|^2}(x) = \exp(-x), \quad x\geqslant 0, \quad (41)$$

$$F_{|h|^2}(x) = 1-\exp(-x), \quad x\geqslant 0. \quad (42)$$

Then, the AOP from (40) becomes

$$\mathcal{P}_{\mathrm{out}}^{\mathrm{AFR}} = 1-\int_0^{\infty}\exp(-\Delta)\exp\left(-z-\frac{X_{\mathrm{B}}\gamma_{\mathrm{th}}}{P_{\mathrm{R}}}\right)dz = 1-\exp\left(-\frac{X_{\mathrm{B}}\gamma_{\mathrm{th}}}{P_{\mathrm{R}}}-\frac{(X_{\mathrm{R}}P_{\mathrm{R}}+X_{\mathrm{B}}P_{\mathrm{B}})\gamma_{\mathrm{th}}}{P_{\mathrm{A}}P_{\mathrm{R}}}\right) \times\int_0^{\infty}\exp\left(-\frac{X_{\mathrm{B}}(X_{\mathrm{R}}P_{\mathrm{R}}+X_{\mathrm{B}}P_{\mathrm{B}})\gamma_{\mathrm{th}}^2+X_{\mathrm{R}}X_{\mathrm{B}}P_{\mathrm{R}}\gamma_{\mathrm{th}}}{zP_{\mathrm{A}}P_{\mathrm{R}}^2}-z\right)dz. \quad (43)$$

Applying [36, Eq. (3.324.1)], the integral in (43) is computed as

$$\int_0^{\infty}\exp\left(-\frac{X_{\mathrm{B}}(X_{\mathrm{R}}P_{\mathrm{R}}+X_{\mathrm{B}}P_{\mathrm{B}})\gamma_{\mathrm{th}}^2+X_{\mathrm{R}}X_{\mathrm{B}}P_{\mathrm{R}}\gamma_{\mathrm{th}}}{zP_{\mathrm{A}}P_{\mathrm{R}}^2}-z\right)dz = 2\sqrt{\frac{X_{\mathrm{B}}(X_{\mathrm{R}}P_{\mathrm{R}}+X_{\mathrm{B}}P_{\mathrm{B}})\gamma_{\mathrm{th}}^2+X_{\mathrm{R}}X_{\mathrm{B}}P_{\mathrm{R}}\gamma_{\mathrm{th}}}{P_{\mathrm{A}}P_{\mathrm{R}}^2}} \times\mathcal{K}_1\left(2\sqrt{\frac{X_{\mathrm{B}}(X_{\mathrm{R}}P_{\mathrm{R}}+X_{\mathrm{B}}P_{\mathrm{B}})\gamma_{\mathrm{th}}^2+X_{\mathrm{R}}X_{\mathrm{B}}P_{\mathrm{R}}\gamma_{\mathrm{th}}}{P_{\mathrm{A}}P_{\mathrm{R}}^2}}\right). \quad (44)$$

Replacing (44) into (43), we obtain the AOP of the TW-FD-AFR system as (39) in Theorem 3.

2) AVERAGE SYMBOL ERROR RATE ANALYSIS

Similar to the ASER of the TW-FD-RIS system, the ASER of the TW-FD-AFR system can be calculated

$$\mathrm{SER}_{\mathrm{B}}^{\mathrm{AFR}} = \frac{\alpha\sqrt{\beta}}{2\sqrt{2\pi}}\int_0^{\infty}\frac{\exp\left(-\frac{\beta x}{2}\right)}{\sqrt{x}}F_{\gamma_{\mathrm{B}}^{\mathrm{AFR}}}(x)dx. \quad (45)$$

Then, the ASER of the TW-FD-AFR system is derived in the following Theorem 4.

Theorem 4: The ASER of the TW-FD-AFR system over Rayleigh fading channels is approximated as

$$\mathrm{SER}_{\mathrm{B}}^{\mathrm{AFR}} \approx \frac{\alpha\sqrt{\beta}}{2\sqrt{2\pi}}\left[\sqrt{\frac{2\pi}{\beta}}-\sqrt{\frac{\pi}{\frac{\beta}{2}+\frac{X_{\mathrm{R}}P_{\mathrm{R}}+X_{\mathrm{B}}P_{\mathrm{A}}+X_{\mathrm{B}}P_{\mathrm{B}}}{P_{\mathrm{A}}P_{\mathrm{R}}}}}\right]. \quad (46)$$

Proof: Similar to the CDF of $\gamma_{\mathrm{B}}^{\mathrm{RIS}}$, the CDF of $\gamma_{\mathrm{B}}^{\mathrm{AFR}}$, $F_{\gamma_{\mathrm{B}}^{\mathrm{AFR}}}(x)$ is given by

$$F_{\gamma_{\mathrm{B}}^{\mathrm{AFR}}}(x) = 1-2\exp\left(-\frac{(X_{\mathrm{R}}P_{\mathrm{R}}+X_{\mathrm{B}}P_{\mathrm{A}}+X_{\mathrm{B}}P_{\mathrm{B}})x}{P_{\mathrm{A}}P_{\mathrm{R}}}\right)$$

$$\times \sqrt{\frac{X_{\rm B}(X_{\rm R}P_{\rm R}+X_{\rm B}P_{\rm B})x^2+X_{\rm R}X_{\rm B}P_{\rm R}x}{P_{\rm A}P_{\rm R}^2}} \times \mathcal{K}_1\left(2\sqrt{\frac{X_{\rm B}(X_{\rm R}P_{\rm R}+X_{\rm B}P_{\rm B})x^2+X_{\rm R}X_{\rm B}P_{\rm R}x}{P_{\rm A}P_{\rm R}^2}}\right). \quad (47)$$

In high SNR regime, the term $\frac{X_{\rm B}(X_{\rm R}P_{\rm R}+X_{\rm B}P_{\rm B})x^2+X_{\rm R}X_{\rm B}P_{\rm R}x}{P_{\rm A}P_{\rm R}^2}$ is very small. Applying the approximation of Bessel function, i.e., $\mathcal{K}_1(u) \approx 1/u$, $F_{\gamma_{\rm B}^{\rm AFR}}(x)$ in (47) is expressed as

$$F_{\gamma_{\rm B}^{\rm AFR}}(x) \approx 1-\exp\left(-\frac{(X_{\rm R}P_{\rm R}+X_{\rm B}P_{\rm A}+X_{\rm B}P_{\rm B})x}{P_{\rm A}P_{\rm R}}\right). \quad (48)$$

Plugging (48) into (45), the ASER of the TW-FD-AFR system is computed as

$$\begin{aligned}{\rm SER}_{\rm B}^{\rm AFR} &\approx \frac{\alpha\sqrt{\beta}}{2\sqrt{2\pi}}\left[\int_0^\infty \frac{\exp\left(-\frac{\beta x}{2}\right)}{\sqrt{x}}dx - \int_0^\infty \frac{\exp\left(-\frac{\beta x}{2}-\frac{(X_{\rm R}P_{\rm R}+X_{\rm B}P_{\rm A}+X_{\rm B}P_{\rm B})x}{P_{\rm A}P_{\rm R}}\right)}{\sqrt{x}}dx\right]\\ &= \frac{\alpha\sqrt{\beta}}{2\sqrt{2\pi}}\left[\sqrt{\frac{2\pi}{\beta}} - \int_0^\infty \frac{\exp\left(-x\left(\frac{\beta}{2}-\frac{(X_{\rm R}P_{\rm R}+X_{\rm B}P_{\rm A}+X_{\rm B}P_{\rm B})}{P_{\rm A}P_{\rm R}}\right)\right)}{\sqrt{x}}dx\right]. \end{aligned} \quad (49)$$

Utilizing [36, Eq. (3.361.2)], the integral in (49) can be solved as

$$\int_0^\infty \frac{\exp\left(-x\left(\frac{\beta}{2}-\frac{(X_{\rm R}P_{\rm R}+X_{\rm B}P_{\rm A}+X_{\rm B}P_{\rm B})}{P_{\rm A}P_{\rm R}}\right)\right)}{\sqrt{x}}dx = \sqrt{\frac{\pi}{\frac{\beta}{2}+\frac{X_{\rm R}P_{\rm R}+X_{\rm B}P_{\rm A}+X_{\rm B}P_{\rm B}}{P_{\rm A}P_{\rm R}}}}. \quad (50)$$

Substituting (50) into (49), we obtain the ASER of the TW-FD-AFR system as (46) in Theorem 4.

3) ASYMPTOTIC SINR

Similar to the TW-FD-RIS system, for the TW-FD-AFR system, the asymptotic expression of the SINR at B in the high SNR regime is calculated as (51), as shown at the bottom of the page.

As shown in (51), in the high SNR regime, the end-to-end SINR at B of the TW-FD-AFR system is a constant and only depends on the residual SI levels at R and B ($k_{\rm R}^2$ and $k_{\rm B}^2$). Thus, the AOP and ASER of the TW-FD-AFR system are constants in the high SNR regime.

IV. NUMERICAL RESULTS AND DISCUSSIONS

This section uses mathematical expressions in previous section to investigate the AOP and ASER of the TW-FD-RIS system in comparison with those of the TW-FD-AFR system. Monte-Carlo simulations are also provided to verify all the derived mathematical expressions. Unless otherwise stated, all the system parameters are set as follows: the average transmission power of A, R and B are $P_{\rm A}=P_{\rm R}=P_{\rm B}=P$; the variances of Gaussian noises are $\sigma_{\rm A}^2=\sigma_{\rm R}^2=\sigma_{\rm B}^2=\sigma^2$; the residual SI levels are $k_{\rm A}^2=k_{\rm R}^2=k_{\rm B}^2=k^2$; and the average SNR is defined as ${\rm SNR}=P/\sigma^2$.

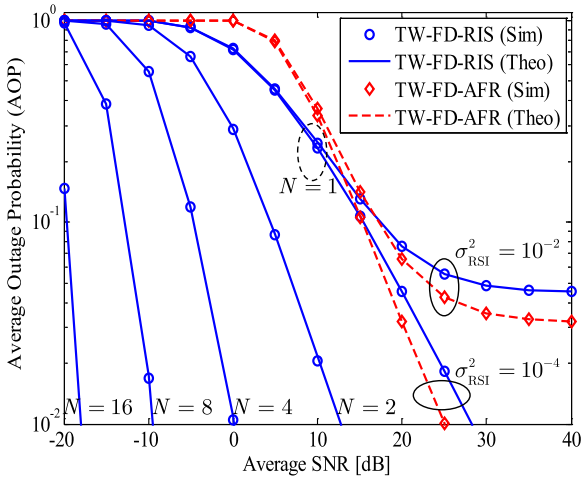

FIGURE 3. The AOPs of TW-FD-RIS and TW-FD-AFR systems versus the average SNR for two residual SI levels, $k^2=10^{-2}$ and 10^{-4}, $\mathcal{R}=1$ bpcu.

Fig. 3 shows the AOPs of TW-FD-RIS and TW-FD-AFR systems versus the average SNR for two residual SI levels,

$$\begin{aligned}\lim_{{\rm SNR}\to\infty}\gamma_{\rm B}^{\rm AFR} &= \lim_{{\rm SNR}\to\infty}\frac{|h_{\rm AR}|^2|h_{\rm RB}|^2P_{\rm A}P_{\rm R}}{|h_{\rm AR}|^2\,X_{\rm B}P_{\rm A}+|h_{\rm RB}|^2(X_{\rm R}P_{\rm R}+X_{\rm B}P_{\rm B})+X_{\rm R}X_{\rm B}}\\ &= \lim_{{\rm SNR}\to\infty}\frac{|h_{\rm AR}|^2|h_{\rm RB}|^2P_{\rm A}P_{\rm R}}{|h_{\rm AR}|^2(k_{\rm B}^2\,P_{\rm B}+\sigma_{\rm B}^2)P_{\rm A}+|h_{\rm RB}|^2[(k_{\rm R}^2\,P_{\rm R}+\sigma_{\rm R}^2)P_{\rm R}+(k_{\rm B}^2\,P_{\rm B}+\sigma_{\rm B}^2)P_{\rm B}]+(k_{\rm R}^2\,P_{\rm R}+\sigma_{\rm R}^2)(k_{\rm B}^2\,P_{\rm B}+\sigma_{\rm B}^2)}\\ &= \lim_{{\rm SNR}\to\infty}\frac{|h_{\rm AR}|^2|h_{\rm RB}|^2{\rm SNR}^2}{|h_{\rm AR}|^2(k_{\rm B}^2{\rm SNR}+1){\rm SNR}+|h_{\rm RB}|^2[(k_{\rm R}^2{\rm SNR}+1){\rm SNR}+(k_{\rm B}^2{\rm SNR}+1){\rm SNR}]+(k_{\rm R}^2{\rm SNR}+1)(k_{\rm B}^2{\rm SNR}+1)}\\ &= \frac{1}{k_{\rm B}^2+k_{\rm R}^2+k_{\rm B}^2+k_{\rm R}^2\,k_{\rm B}^2} \end{aligned} \quad (51)$$

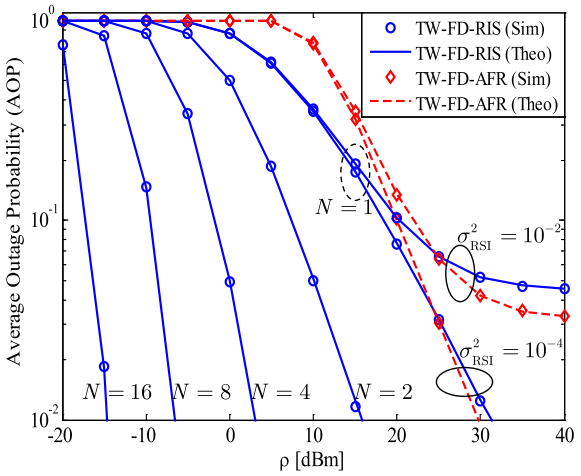

FIGURE 4. The AOPs of the TW-FD-RIS and TW-FD-AFR systems versus the total average transmission power for two residual SI levels, $k^2 = 10^{-2}$ and 10^{-4}, $\mathcal{R} = 1$ bpcu.

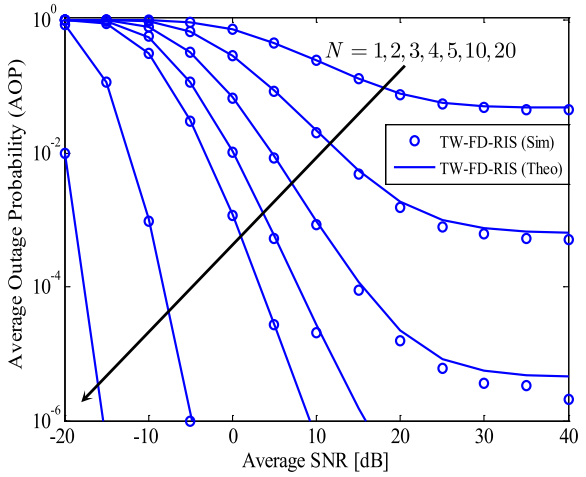

FIGURE 5. The impact of the number of elements of RIS, N, on the AOP of the TW-FD-RIS system for $k^2 = 10^{-2}$.

$k^2 = 10^{-2}$ and $k^2 = 10^{-4}$. The predefined data transmission rate is $\mathcal{R} = 1$ bit per channel use (bpcu). We use (21) and (23) to plot the AOPs of the TW-FD-RIS system for $N = 2$ and $N = 1$, respectively. Meanwhile, (39) is used to plot the AOPs of the TW-FD-AFR system. Importantly, in Fig. 3, we set $P_A = P_R = P_B = P$ for the TW-FD-AFR system while $P_A = P_B = P$ for the TW-FD-RIS system. These settings lead to the total transmission power of the TW-FD-AFR system is higher than that of the TW-FD-RIS system. As observed from Fig. 3, in the case $N = 1$, the AOPs of the TW-FD-RIS system are lower or higher than those of the TW-FD-AFR system. Particularly, the AOPs of the TW-FD-RIS system with $N = 1$ are lower when SNR $<$ 15 dB and are higher when SNR $>$ 15 dB. As N increases, i.e., $N = 2$, the AOPs of the TW-FD-RIS system significantly reduce. Specifically, when $N = 2$ and SNR = 12 dB, the AOPs of the TW-FD-RIS system are approximately 10^{-2} for both $k^2 = 10^{-2}$ and $k^2 = 10^{-4}$. Meanwhile, when $N = 1$ and SNR = 12 dB, the AOPs of the TW-FD-RIS system are approximately 10^{-1} for both $k^2 = 10^{-2}$ and $k^2 = 10^{-4}$. These features demonstrate the benefits of employing RIS to improve the performance of wireless systems. On the other hand, in the case of high residual SI level ($k^2 = 10^{-2}$), both AOPs of the TW-FD-AFR and TW-FD-RIS systems with $N = 1$ reach the error floors in high SNR regime because of the impact of residual SI (refers to (37) and (51)).

Fig. 4 compares the AOPs of the TW-FD-RIS and TW-FD-AFR systems with similar total transmission power. Other parameters to obtain Fig. 4 are similar to those in Fig. 3. For Fig. 4, we set the total transmission power, $\rho = P_A + P_B$ for the TW-FD-RIS system and $\rho = P_A + P_R + P_B$ for the TW-FD-AFR system. We observe that although the AOPs of both the TW-FD-RIS and TW-FD-AFR systems in Fig. 4 are higher in comparison with those in Fig. 3, the patterns of the AOP curves are still similar to those in Fig. 3. Specifically, in the case $N = 1$, the AOPs of the TW-FD-RIS system are lower when $\rho < 25$ dBm and higher than those of the TW-FD-AFR system when $\rho > 25$ dBm. Therefore, in the special case, i.e., $N = 1$, we should use the RIS in low transmission power and the AF relay in high transmission power to achieve better performance of the TW-FD system. Note that the RIS in practice can be equipped with many reflecting elements. However, we still use these cases of $N = 1$ and $N = 2$ to emphasize the benefits of using RIS in comparison with using AFR.

Fig. 5 investigates the impact of the number of elements of RIS, N, on the AOP of the TW-FD-RIS system for $k^2 = 10^{-2}$. Specifically, we also use (21) to plot the AOP of the TW-FD-RIS system in the case $N = 1$. We observe that, although (21) is derived for the case $N \geq 2$, it can be used in the case $N = 1$ because the numerical results almost match the simulation results in this case. Furthermore, in the low SNR regime (SNR $<$ 20 dB), (21) can be considered as the exact expression of the AOP of the TW-FD-RIS system. However, in the high SNR regime (SNR $>$ 20 dB), (21) becomes an approximate expression. It is obvious from Fig. 5 that increasing N leads to a significant decrease in the AOP of the TW-FD-RIS system. Specifically, in the high SNR regime (i.e., SNR = 40 dB), the AOPs reach the error floors of 10^{-1}, 10^{-3}, and 10^{-5} for $N = 1$, $N = 2$, and $N = 3$, respectively. In other words, increasing only one element of the RIS (from 1 to 2 or from 2 to 3) makes the AOP of the TW-FD-RIS system reduce 100 times. If N still increases, i.e., $N = 4, 5, 10, 20$, the AOP rapidly reduces and avoids the error floor. In summary, the usage of RIS with larger elements ($N \geq 4$) greatly reduces the impact of the residual SI induced by FD mode and significantly improves the performance of the TW-FD system.

Fig. 6 illustrates the ASERs of the TW-FD-RIS system in comparison with those of the TW-FD-AFR system for three modulation schemes, i.e., BPSK ($\alpha = 1, \beta = 2$), 4-QAM ($\alpha = 2, \beta = 1$), and 8-QAM ($\alpha = 4 - \sqrt{2}, \beta = 3/7$), $N = 1$, and $k^2 = 10^{-4}$. We use (34) and (46) to plot the analysis curves of the ASERs of the TW-FD-RIS and TW-FD-AFR

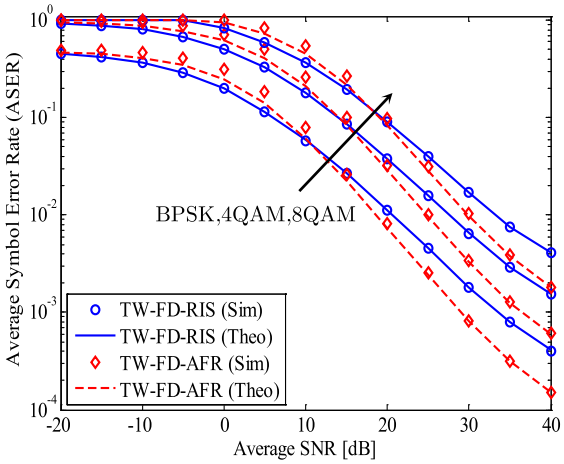

FIGURE 6. The ASERs of the TW-FD-RIS system in comparison with those of the TW-FD-AFR system for three modulation schemes, $N = 1$, $k^2 = 10^{-4}$.

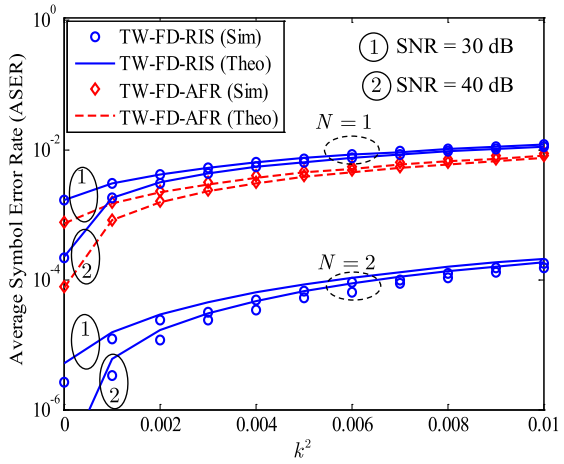

FIGURE 7. The impact of the residual SI level, k^2, on the ASERs of the TW-FD-RIS and TW-FD-AFR systems with BPSK modulation for SNR = 30 and 40 dB.

systems, respectively. Like the AOPs, the ASERs of the TW-FD-RIS system can be lower or higher than those of the TW-FD-AFR system. Specifically, when BPSK is used and SNR = 40 dB, the ASER is 4×10^{-4} for the TW-FD-RIS system while 1.5×10^{-4} for the TW-FD-AFR system. In other words, the ASER performance of the TW-FD-AFR system is nearly three times higher than that of the TW-FD-RIS system. On the other hand, in the high SNR regime, the approximate expression in (46) becomes an exact closed-form expression of the ASER of the TW-FD-AFR system.

Fig. 7 analyzes the impact of the residual SI level, k^2, on the ASERs of the TW-FD-RIS and TW-FD-AFR systems with BPSK modulation for SNR = 30 and 40 dB. Note that we use (27) and (34) to obtain the ASERs of the TW-FD-RIS system in the cases $N = 2$ and $N = 1$, respectively. As shown in Fig. 7, the ASERs of the TW-FD-RIS and TW-FD-AFR systems are greatly affected by residual SI induced by FD transmission mode. Specifically, when $N = 1$ and k^2 increases from 0 to 0.001, the ASERs of the TW-FD-RIS

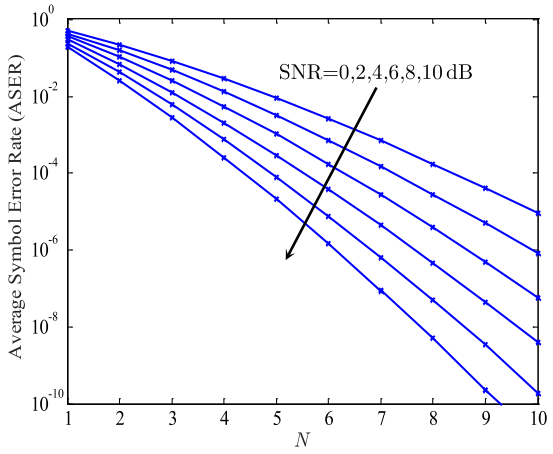

FIGURE 8. The ASERs of the TW-FD-RIS system with 4-QAM modulation versus N for different SNRs, $k^2 = 10^{-2}$.

system increase from 1.7×10^{-3} and 2.1×10^{-4} to 3×10^{-3} and 1.8×10^{-3} for SNR = 30 dB and 40 dB, respectively. In other words, when k^2 increases from 0 to 0.001, the ASERs of the TW-FD-RIS system in the case of $N = 1$ increase 2 times for SNR = 30 dB and 8.5 times for SNR = 40 dB. Meanwhile, the ASERs of the TW-FD-AFR system increase from 8×10^{-4} and 7.5×10^{-5} to 1.5×10^{-3} and 8×10^{-4} for SNR = 30 and 40 dB, respectively. Also, in the high SNR regime, the ASERs of the TW-FD-AFR system are always lower than those of the TW-FD-RIS system when $N = 1$. However, when $N = 2$, the ASERs of the TW-FD-AFR system are significantly higher than those of the TW-FD-RIS system.

Fig. 8 depicts the ASERs of the TW-FD-RIS system with 4-QAM modulation versus the number of the elements of RIS, N, for different SNRs, i.e., SNR = 0, 2, 4, 6, 8, 10 dB, $k^2 = 10^{-2}$. As can be seen from Fig. 8, the diversity order of the TW-FD-RIS system can be considered as a linear function of N. In particular, when N increases from 3 to 4, ASERs reduce from 8.6×10^{-2}, 4.9×10^{-2}, 2.6×10^{-2}, 1.3×10^{-2}, 6.2×10^{-3}, and 2.9×10^{-3} to 3×10^{-2}, 1.3×10^{-2}, 5.5×10^{-3}, 2.1×10^{-3}, 7.6×10^{-4}, and 2.6×10^{-4} for SNR = 0, 2, 4, 6, 8, and 10 dB, respectively. In summary, the ASERs reduce much faster for higher SNR when N increases from 3 to 4. On the other hand, in the case of $N = 9$, the ASERs are 4.1×10^{-5}, 5×10^{-6}, 5×10^{-7}, 4.5×10^{-8}, 3.6×10^{-9}, and 2.2×10^{-10} for SNR = 0, 2, 4, 6, 8, and 10 dB, respectively. In brief, for a certain value of N, when SNR increases 2 dB, the ASER of the TW-FD-RIS system approximately reduces to one tenth of it.

V. CONCLUSION

Motivated by the advantages of RIS and its application in future wireless networks, in this paper, we conducted a mathematical analysis of a TW-FD communication system assisted with a RIS and an AF relay. We successfully derived the approximate expressions of the AOP and the ASER of the TW-FD-RIS system in the case $N \geq 2$ and the exact

closed-form expressions in the case $N = 1$. Furthermore, the exact closed-form expression of the AOP and the approximate expression of the ASER of the TW-FD-AFR system are also obtained for comparison. Numerical results showed that when $N = 1$, the performance of the TW-FD-RIS system was better than that of the TW-FD-AFR system in the low SNR regime, but it was worse in the high SNR regime, even when the total transmission power of the TW-FD-AFR system was higher than that of the TW-FD-RIS system. Additionally, in the case $N \geq 2$, the impact of the residual SI indued by FD mode was significantly reduced. Furthermore, the diversity order of the TW-FD-RIS system was a linear function of N. Therefore, when current techniques cannot perfectly remove the self-interference induced by FD mode, the usage of RIS with a larger number of elements can greatly improve the performance of TW-FD systems.

REFERENCES

[1] S. Atapattu, R. Fan, P. Dharmawansa, G. Wang, J. Evans, and T. A. Tsiftsis, "Reconfigurable intelligent surface assisted two–way communications: Performance analysis and optimization," *IEEE Trans. Commun.*, vol. 68, no. 10, pp. 6552–6567, Oct. 2020.

[2] A.-A.-A. Boulogeorgos and A. Alexiou, "Performance analysis of reconfigurable intelligent surface-assisted wireless systems and comparison with relaying," *IEEE Access*, vol. 8, pp. 94463–94483, 2020.

[3] E. Basar, M. Di Renzo, J. De Rosny, M. Debbah, M.-S. Alouini, and R. Zhang, "Wireless communications through reconfigurable intelligent surfaces," *IEEE Access*, vol. 7, pp. 116753–116773, 2019.

[4] L. Yang, Y. Yang, M. O. Hasna, and M.-S. Alouini, "Coverage, probability of SNR gain, and DOR analysis of RIS-aided communication systems," *IEEE Wireless Commun. Lett.*, vol. 9, no. 8, pp. 1268–1272, Aug. 2020.

[5] H. Zhang, B. Di, L. Song, and Z. Han, "Reconfigurable intelligent surfaces assisted communications with limited phase shifts: How many phase shifts are enough?" *IEEE Trans. Veh. Technol.*, vol. 69, no. 4, pp. 4498–4502, Apr. 2020.

[6] B. Di, H. Zhang, L. Song, Y. Li, Z. Han, and H. V. Poor, "Hybrid beamforming for reconfigurable intelligent surface based multi-user communications: Achievable rates with limited discrete phase shifts," *IEEE J. Sel. Areas Commun.*, vol. 38, no. 8, pp. 1809–1822, Aug. 2020.

[7] K. A. Darabkh, O. M. Amro, H. B. Salameh, and R. T. Al-Zubi, "A—Z overview of the in-band full-duplex cognitive radio networks," *Comput. Commun.*, vol. 145, pp. 66–95, Sep. 2019.

[8] A. H. Gazestani, S. A. Ghorashi, B. Mousavinasab, and M. Shikh-Bahaei, "A survey on implementation and applications of full duplex wireless communications," *Phys. Commun.*, vol. 34, pp. 121–134, Jun. 2019.

[9] H. H. M. Tam, H. D. Tuan, A. A. Nasir, T. Q. Duong, and H. V. Poor, "MIMO energy harvesting in full-duplex multi-user networks," *IEEE Trans. Wireless Commun.*, vol. 16, no. 5, pp. 3282–3297, May 2017.

[10] V. Singh, A. Gadre, and S. Kumar, "Full duplex radios," in *Proc. 19th ACM Workshop Hot Topics Netw.*, Nov. 2020, pp. 375–386.

[11] E. Everett, A. Sahai, and A. Sabharwal, "Passive self-interference suppression for full-duplex infrastructure nodes," *IEEE Trans. Wireless Commun.*, vol. 13, no. 2, pp. 680–694, Feb. 2014.

[12] X. Li, C. Tepedelenlioglu, and H. Senol, "Channel estimation for residual self-interference in full-duplex amplify-and-forward two-way relays," *IEEE Trans. Wireless Commun.*, vol. 16, no. 8, pp. 4970–4983, Aug. 2017.

[13] L. Irio and R. Oliveira, "Distribution of the residual self-interference power in in-band full-duplex wireless systems," *IEEE Access*, vol. 7, pp. 57516–57526, 2019.

[14] M. Di Renzo, K. Ntontin, J. Song, F. H. Danufane, X. Qian, F. Lazarakis, J. De Rosny, D.-T. Phan-Huy, O. Simeone, R. Zhang, M. Debbah, G. Lerosey, M. Fink, S. Tretyakov, and S. Shamai (Shitz), "Reconfigurable intelligent surfaces vs. Relaying: Differences, similarities, and performance comparison," *IEEE Open J. Commun. Soc.*, vol. 1, pp. 798–807, 2020.

[15] Y. Chen, B. Ai, H. Zhang, Y. Niu, L. Song, Z. Han, and H. V. Poor, "Reconfigurable intelligent surface assisted device-to-device communications," *IEEE Trans. Wireless Commun.*, vol. 20, no. 5, pp. 2792–2804, May 2021.

[16] M. A. ElMossallamy, H. Zhang, L. Song, K. G. Seddik, Z. Han, and G. Y. Li, "Reconfigurable intelligent surfaces for wireless communications: Principles, challenges, and opportunities," *IEEE Trans. Cognit. Commun. Netw.*, vol. 6, no. 3, pp. 990–1002, Sep. 2020.

[17] A. Hemanth, K. Umamaheswari, A. C. Pogaku, D.-T. Do, and B. M. Lee, "Outage performance analysis of reconfigurable intelligent surfaces-aided NOMA under presence of hardware impairment," *IEEE Access*, vol. 8, pp. 212156–212165, 2020.

[18] T. Hou, Y. Liu, Z. Song, X. Sun, and Y. Chen, "MIMO-NOMA networks relying on reconfigurable intelligent surface: A signal cancellation-based design," *IEEE Trans. Commun.*, vol. 68, no. 11, pp. 6932–6944, Nov. 2020.

[19] T. Hou, Y. Liu, Z. Song, X. Sun, Y. Chen, and L. Hanzo, "Reconfigurable intelligent surface aided NOMA networks," *IEEE J. Sel. Areas Commun.*, vol. 38, no. 11, pp. 2575–2588, Nov. 2020.

[20] C. Zhang, W. Yi, Y. Liu, Z. Qin, and K. K. Chai, "Downlink analysis for reconfigurable intelligent surfaces aided NOMA networks," in *Proc. GLOBECOM IEEE Global Commun. Conf.*, Dec. 2020, pp. 1–6.

[21] M. Jung, W. Saad, Y. Jang, G. Kong, and S. Choi, "Reliability analysis of large intelligent surfaces (LISs): Rate distribution and outage probability," *IEEE Wireless Commun. Lett.*, vol. 8, no. 6, pp. 1662–1666, Dec. 2019.

[22] S. Lin, B. Zheng, G. C. Alexandropoulos, M. Wen, M. Di Renzo, and F. Chen, "Reconfigurable intelligent surfaces with reflection pattern modulation: Beamforming design and performance analysis," *IEEE Trans. Wireless Commun.*, vol. 20, no. 2, pp. 741–754, Feb. 2021.

[23] W. Mei and R. Zhang, "Cooperative beam routing for multi-IRS aided communication," *IEEE Wireless Commun. Lett.*, vol. 10, no. 2, pp. 426–430, Feb. 2021.

[24] K. O. Odeyemi, P. A. Owolawi, and O. O. Olakanmi, "Reconfigurable intelligent surface assisted mobile network with randomly moving user over Fisher-Snedecor fading channel," *Phys. Commun.*, vol. 43, Dec. 2020, Art. no. 101186.

[25] P. K. Sharma and P. Garg, "Intelligent reflecting surfaces to achieve the full-duplex wireless communication," *IEEE Commun. Lett.*, vol. 25, no. 2, pp. 622–626, Feb. 2021.

[26] Y. Cai, M. Zhao, K. Xu, and R. Zhang, "Intelligent reflecting surface aided full-duplex communication: Passive beamforming and deployment design," 2020, *arXiv:2012.07218*. [Online]. Available: https://arxiv.org/abs/2012.07218

[27] Z. Peng, Z. Zhang, C. Pan, L. Li, and A. L. Swindlehurst, "Multiuser full-duplex two-way communications via intelligent reflecting surface," *IEEE Trans. Signal Process.*, vol. 69, pp. 837–851, 2021.

[28] C. Li, Z. Chen, Y. Wang, Y. Yao, and B. Xia, "Outage analysis of the full-duplex decode-and-forward two-way relay system," *IEEE Trans. Veh. Technol.*, vol. 66, no. 5, pp. 4073–4086, May 2017.

[29] C. Li, B. Xia, S. Shao, Z. Chen, and Y. Tang, "Multi-user scheduling of the full-duplex enabled two-way relay systems," *IEEE Trans. Wireless Commun.*, vol. 16, no. 2, pp. 1094–1106, Feb. 2017.

[30] B. C. Nguyen, X. N. Tran, L. V. Nguyen, and L. T. Dung, "On the performance of full-duplex spatial modulation MIMO system with and without transmit antenna selection under imperfect hardware conditions," *IEEE Access*, vol. 8, pp. 185218–185231, 2020.

[31] B. C. Nguyen, X. N. Tran, D. T. Tran, X. N. Pham, and L. T. Dung, "Impact of hardware impairments on the outage probability and ergodic capacity of one-way and two-way full-duplex relaying systems," *IEEE Trans. Veh. Technol.*, vol. 69, no. 8, pp. 8555–8567, Aug. 2020.

[32] D. Kudathanthirige, D. Gunasinghe, and G. Amarasuriya, "Performance analysis of intelligent reflective surfaces for wireless communication," in *Proc. IEEE Int. Conf. Commun. (ICC)*, Jun. 2020, pp. 1–6.

[33] H. Cui, M. Ma, L. Song, and B. Jiao, "Relay selection for two-way full duplex relay networks with amplify-and-forward protocol," *IEEE Trans. Wireless Commun.*, vol. 13, no. 7, pp. 3768–3777, Jul. 2014.

[34] A. Goldsmith, *Wireless Communications*. Cambridge, U.K.: Cambridge Univ. Press, 2005.

[35] B. C. Nguyen, T. M. Hoang, and L. T. Dung, "Performance analysis of vehicle-to-vehicle communication with full-duplex amplify-and-forward relay over double-Rayleigh fading channels," *Veh. Commun.*, vol. 19, Oct. 2019, Art. no. 100166.

[36] A. Jeffrey and D. Zwillinger, *Table of Integrals, Series, and Products*. New York, NY, USA: Academic, 2007.

[37] M. Abramowitz and I. A. Stegun, *Handbook of Mathematical Functions With Formulas, Graphs, and Mathematical Tables*, vol. 9. New York, NY, USA: Dover, 1972.

BA CAO NGUYEN received the B.S. degree from Telecommunication University, Nha Trang, Vietnam, in 2006, the M.S. degree from the Posts and Telecommunications Institute of Technology (VNPT), Ho Chi Minh City, Vietnam, in 2011, and the Ph.D. degree from Le Quy Don Technical University, Hanoi, Vietnam, in 2020. From November 2019 to April 2021, he works as a Lecturer with Telecommunications University. Since May 2021, he has been with Chungbuk National University, as a Postdoctoral Research Fellow. His research interests include energy harvesting, full-duplex, spatial modulation, NOMA, MIMO, RIS, and cooperative communication.

TRAN MANH HOANG received the B.S. degree in communication command from Telecommunications University, Ministry of Defense, Nha Trang, Vietnam, in 2002, the B.Eng. degree in electrical engineering from Le Quy Don Technical University, Hanoi, Vietnam, in 2006, the M.Eng. degree in electronics engineering from the Posts and Telecommunications Institute of Technology (VNPT), Vietnam, in 2013, and the Ph.D. degree from Le Quy Don Technical University. He is currently a Lecturer with Telecommunications University. His research interests include energy harvesting, non-orthogonal multiple access, and signal processing for wireless cooperative communications.

LE THE DUNG (Member, IEEE) received the B.S. degree in electronics and telecommunication engineering from the Ho Chi Minh City University of Technology, Ho Chi Minh City, Vietnam, in 2008, and the M.S. and Ph.D. degrees in electronics and computer engineering from Hongik University, Seoul, South Korea, in 2012 and 2016, respectively. From 2007 to 2010, he joined Signet Design Solutions Vietnam Company Ltd., as a Hardware Design Engineer. Since May 2016, he has been with Chungbuk National University, as a Postdoctoral Research Fellow. He has more than 60 articles in refereed international journals and papers in conferences. His major research interests include routing protocols, network coding, network stability analysis and optimization in mobile ad-hoc networks, cognitive radio *ad-hoc* networks, and visible light communication networks. He was a recipient of the IEEE IS3C2016 Best Paper Award.

TAEJOON KIM (Member, IEEE) received the B.S. degree in electronics engineering from Yonsei University, Seoul, Republic of Korea, in 2003, and the Ph.D. degree in electrical engineering from the Korea Advanced Institute of Science and Technology (KAIST), Daejeon, Republic of Korea, in 2011. From 2003 to 2005, he was a Researcher with LG Electronics, Seoul. From 2011 to 2013, he was a Senior Researcher with Electronics and Telecommunications Research Institute (ETRI), Daejeon. He is currently an Associate Professor with the School of Information and Communication Engineering, Chungbuk National University, Chungju, Republic of Korea. His research interests include communication theory and analysis, and optimization of wireless networks.